XXV International Baldin Seminar
on High Energy Physics Problems 2023

STAR experiment results from BES program

Artem Korobitsin for the STAR collaboration
Joint Institute for Nuclear Research

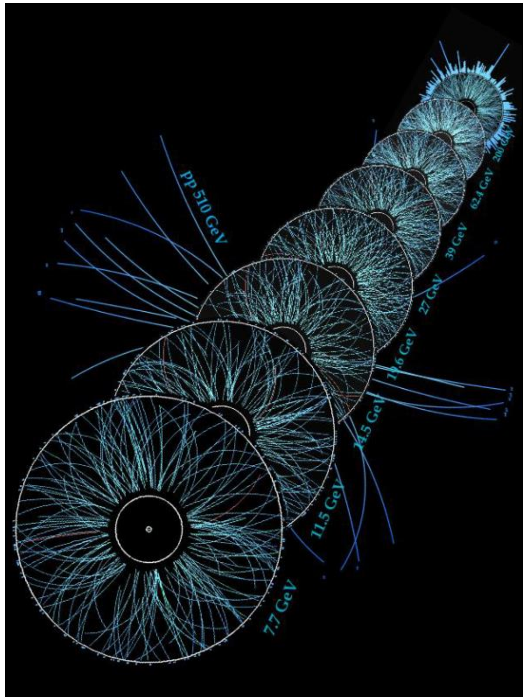

Supported in part by
U.S. DEPARTMENT OF ENERGY

XXV ISHEPP, September 18 - 23, Dubna, Russia

Part of this work was supported by Russian Science Foundation under grant №22-72-10028

Outline:

- *Introduction*
- *The STAR experiment*
- *Femtoscopy*
- *Flow fluctuation*
- *Hyper-nuclei*
- *Rapidity Dependent Spectra*
- *Global polarization*
- R_{cp} *in high* p_T *region*
- *Summary*

Beam Energy Scan to map the QCD phase diagram

Two stages of Beam Energy Scan:

BES-I: 7.7 – 39 GeV (2010 – 2014)

- Search for the QGP turn-off signatures
- Search for the first-order phase transition
- Search for the critical point

First glance at low energy region, rather low statistics

BES-II and fixed-target (FXT) program:

3.0 – 54.4 GeV (2017 – 2021)

- Detector upgrades (increased acceptance and PID capabilities)
- Access to energies $\sqrt{s_{NN}}$ < 7.7 GeV via FXT

Precise measurements at low energies, large statistics

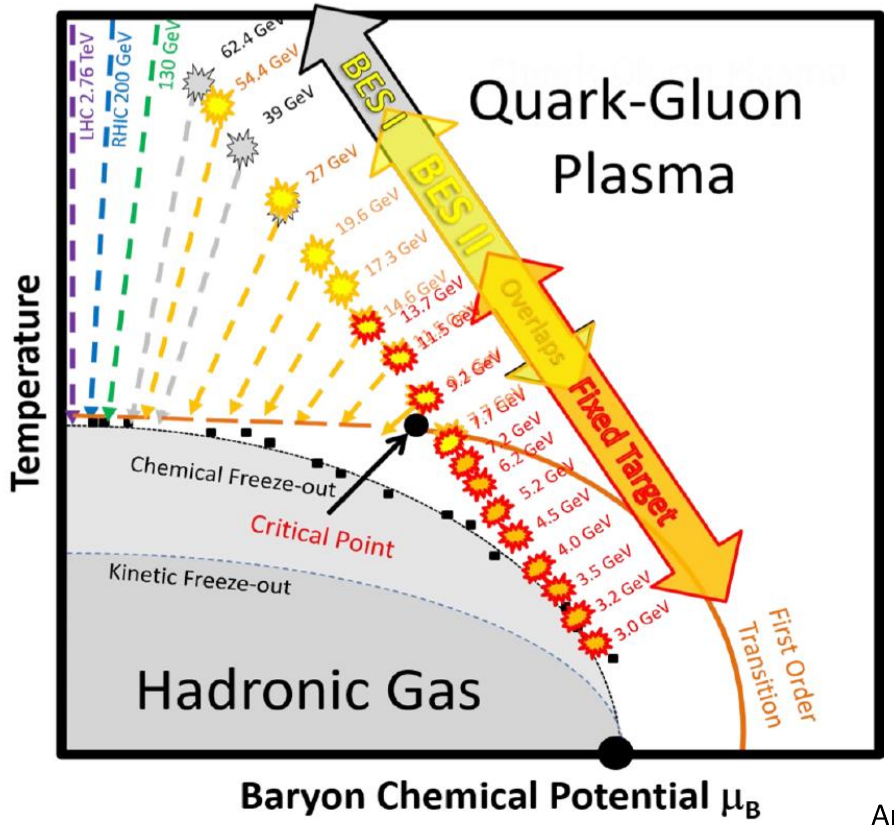

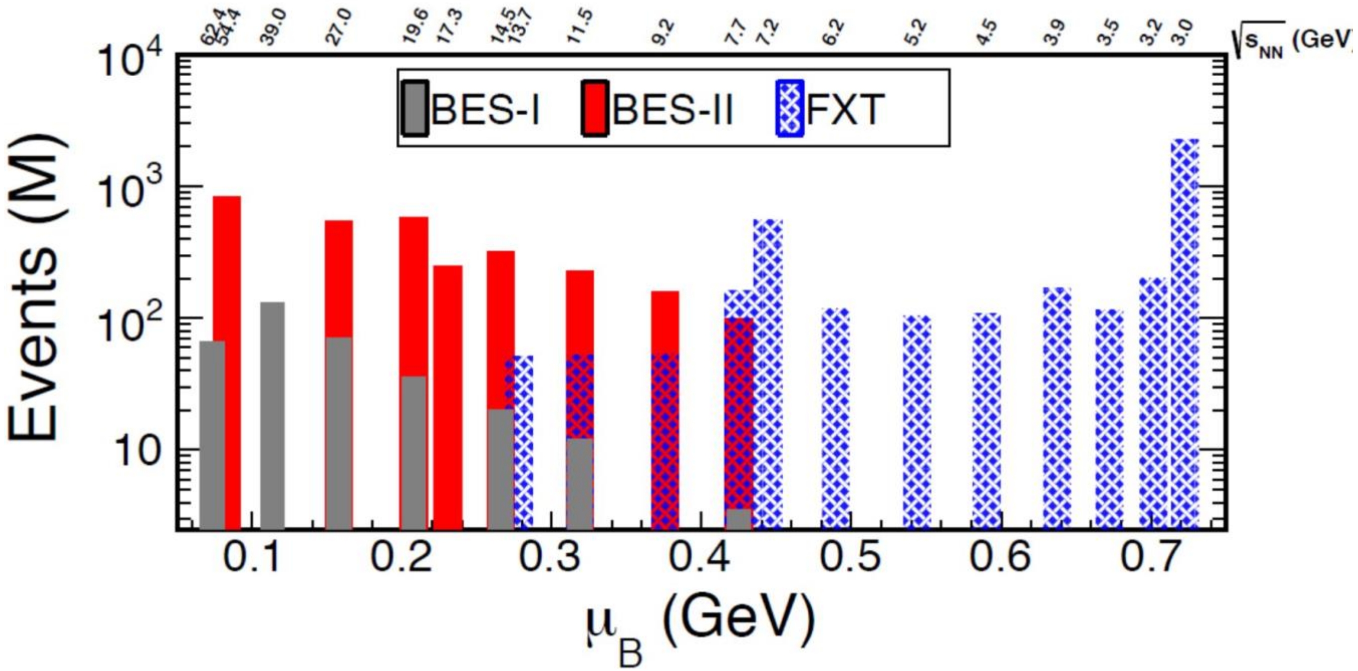

Relativistic Heavy Ion Collider (RHIC)

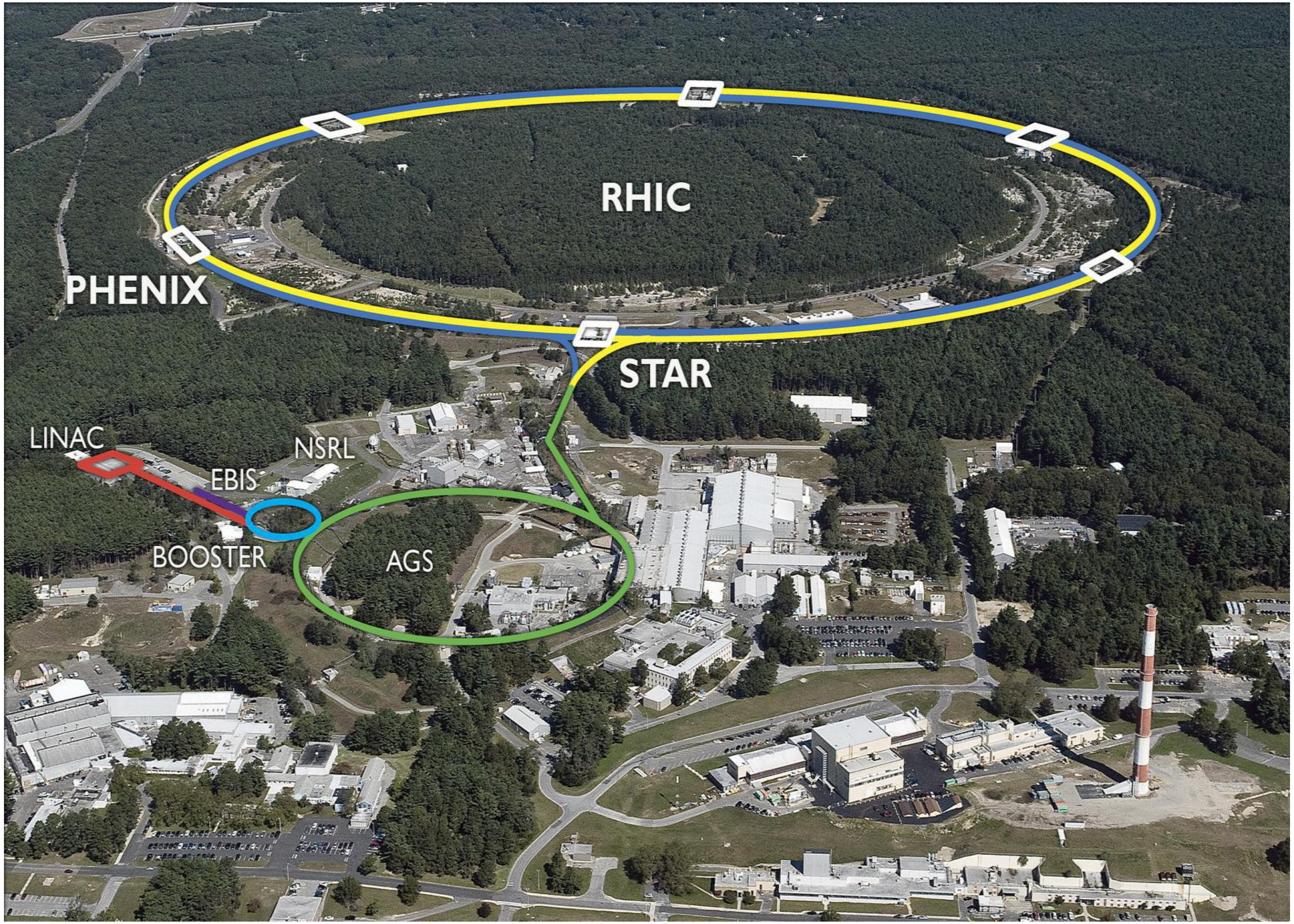

In operation since 1999

3.83 km circumference

Suitable for p+p, p+A, A+A

Max. colliding energy:
200 GeV for Au+Au
510 GeV for p+p

Exploring QCD matter and its phase boundary. Different colliding systems (Au+Au, U+U, p+Al, p+Au, d+Au, 3He+Au, Cu+Au, Cu+Cu, Al+Au, Zr+Zr, Ru+Ru) and energies.

Spin physics on polarized proton beams

Solenoidal Tracker At RHIC (STAR detector)

Tracking and PID (full 2π)

TPC: $|\eta| < 1$
iTPC (2019+): $|\eta| < 1.5$:
(extended η acceptance, improved tracking, better dE/dx resolution, better momentum resolution)
TOF: $|\eta| < 1$
eTOF (2019+): $-1.6 < \eta < -1$
(extend forward PID capability)
BEMC: $|\eta| < 1$
EEMC: $1 < \eta < 2$
HFT (2014-2016): $|\eta| < 1$
MTD (2014+): $|\eta| < 0.5$
(partial azimuthal coverage)

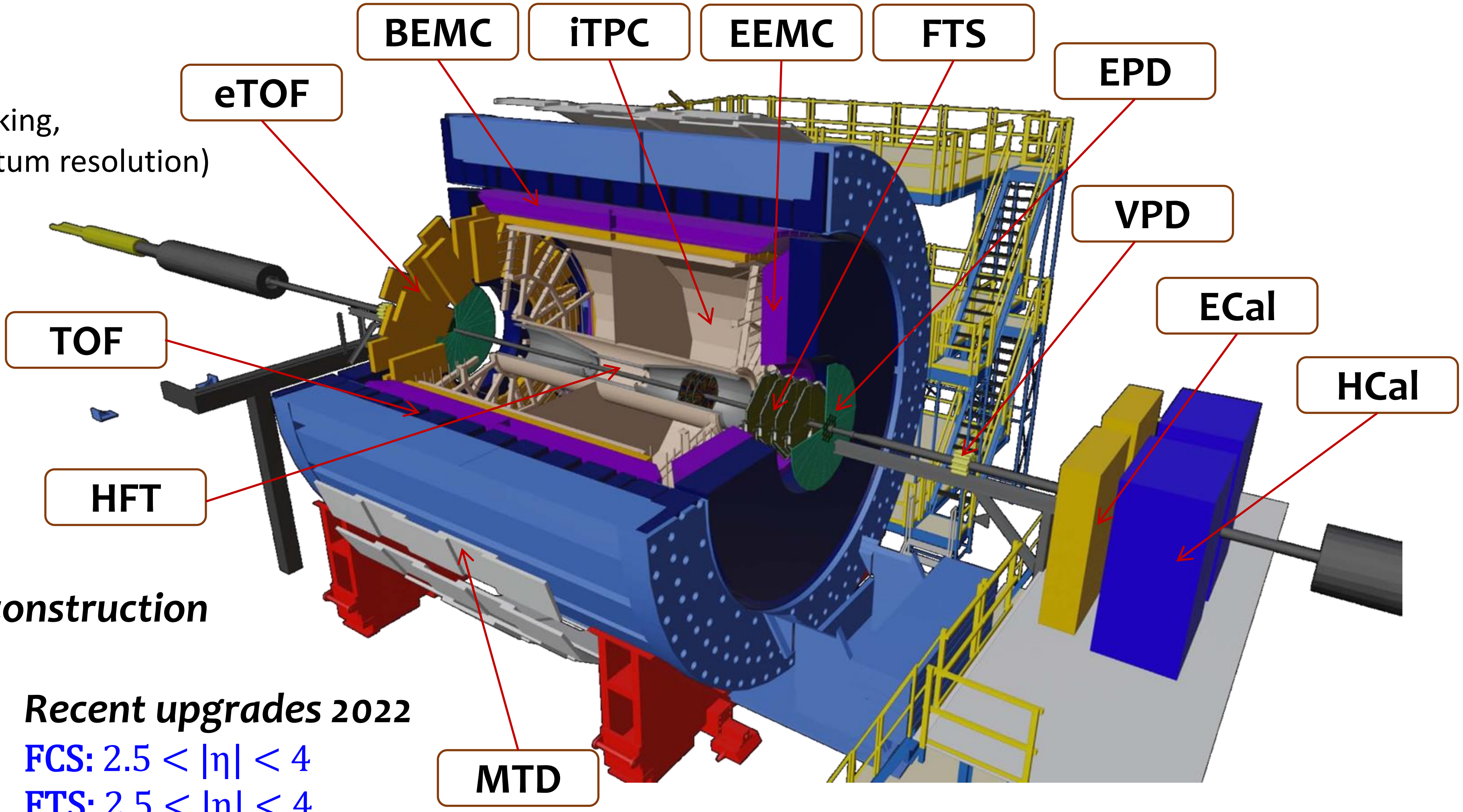

MB trigger and event plane reconstruction

BBC (before 2018): $3.3 < |\eta| < 5$
EPD (2018+): $2.1 < |\eta| < 5.1$
(better EP resolution compared to BBC)
VPD: $4.2 < |\eta| < 5$
ZDC: $6.5 < |\eta| < 7.5$

Recent upgrades 2022

FCS: $2.5 < |\eta| < 4$
FTS: $2.5 < |\eta| < 4$
ECAL & HCAL : $2.5 < |\eta| < 4$

The Fixed-target (FXT) Setup

$$\eta = \frac{1}{2}\ln\left(\frac{|\mathbf{p}| + p_L}{|\mathbf{p}| - p_L}\right)$$

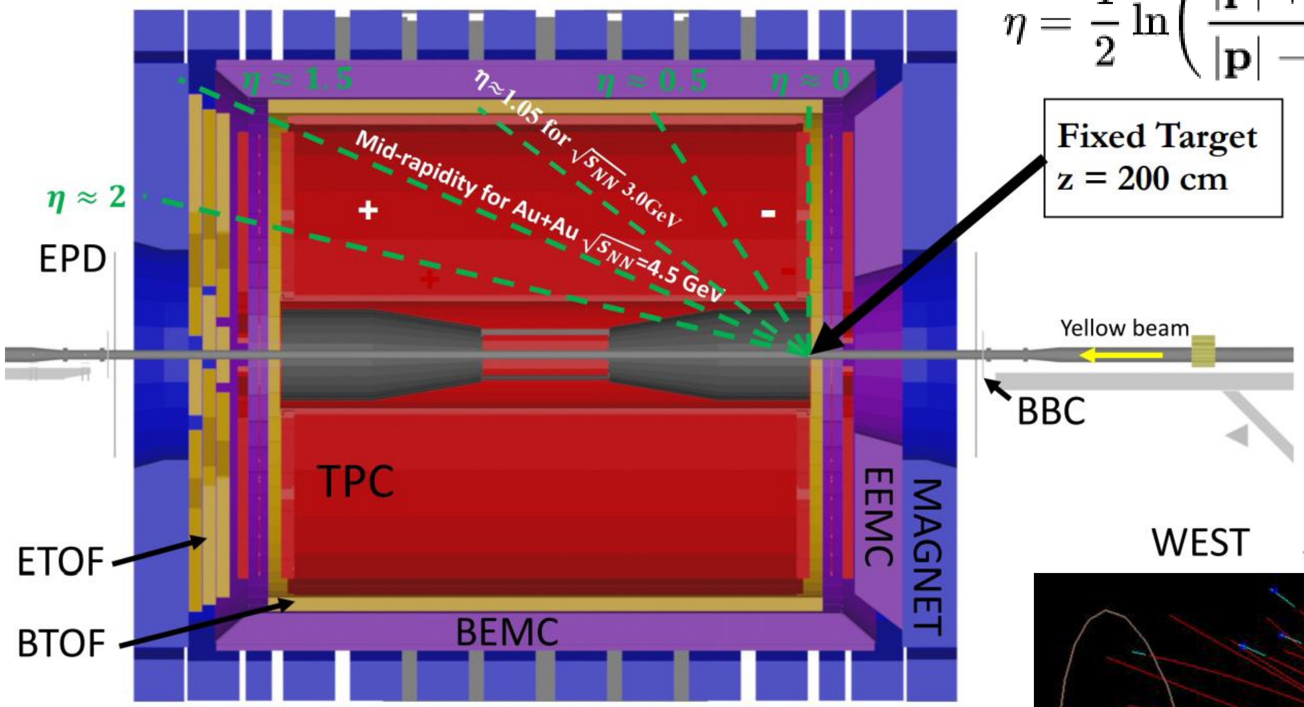

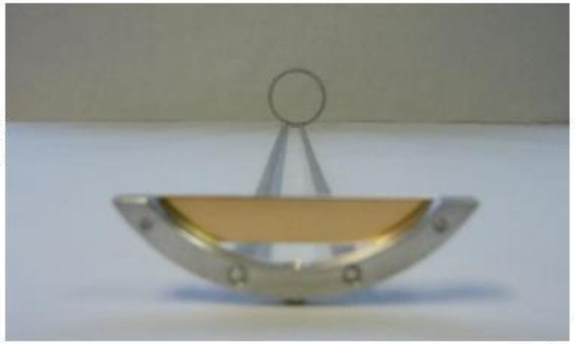

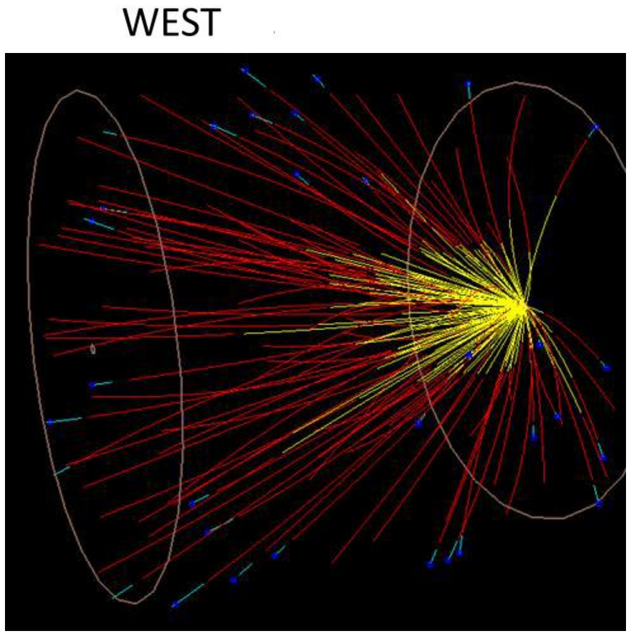

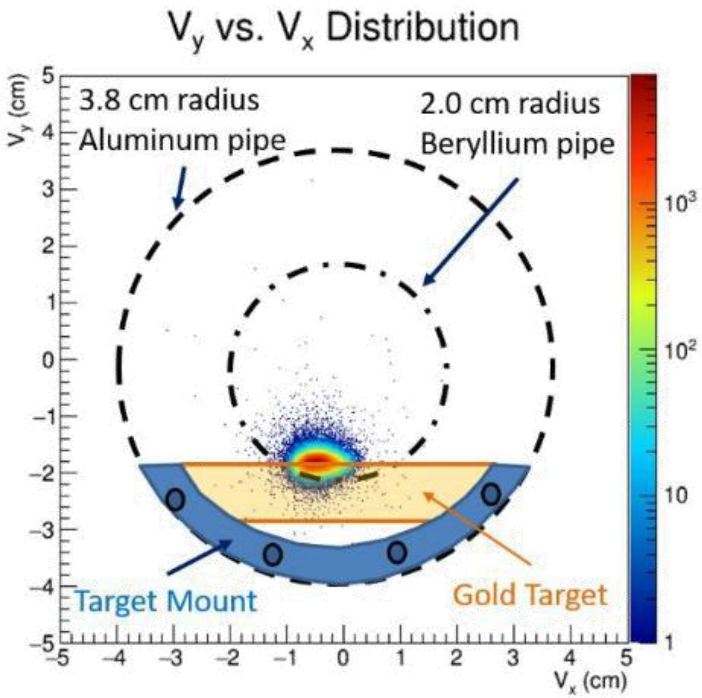

Gold target:

- 2 cm below nominal beam axis
- 2 m from center of STAR
- 0.25 mm foil

Particle identification at 3 GeV

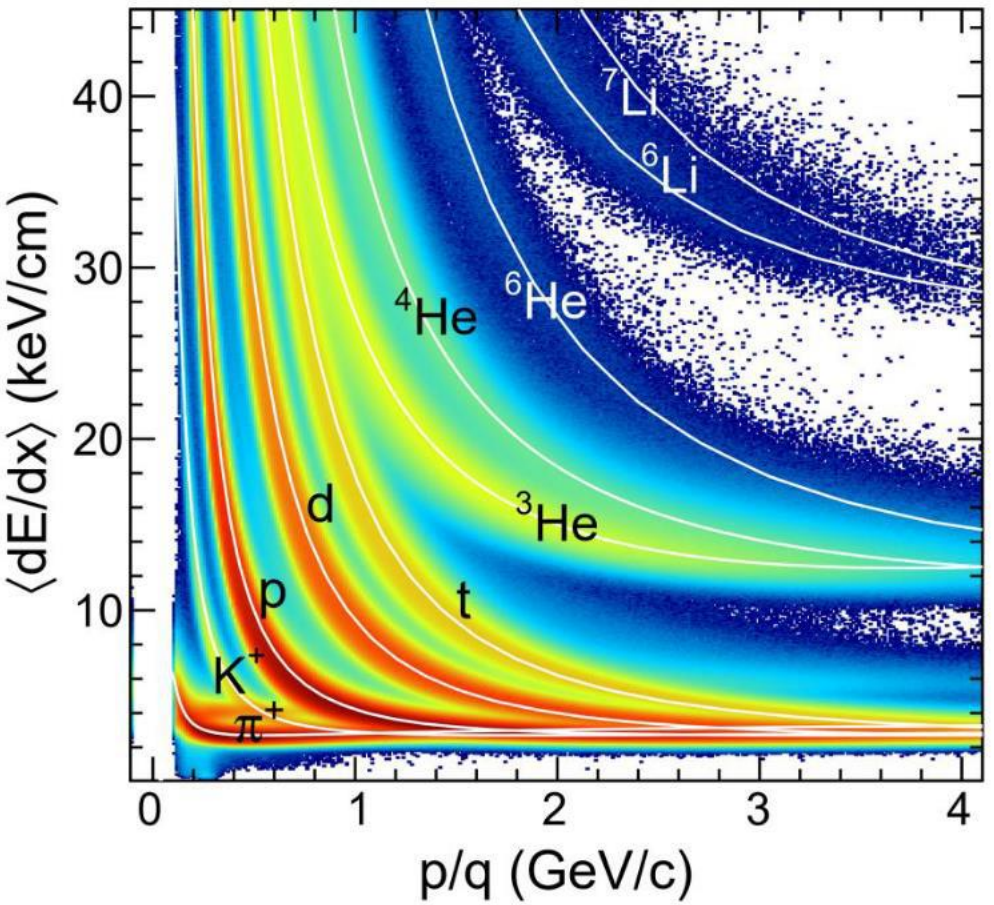

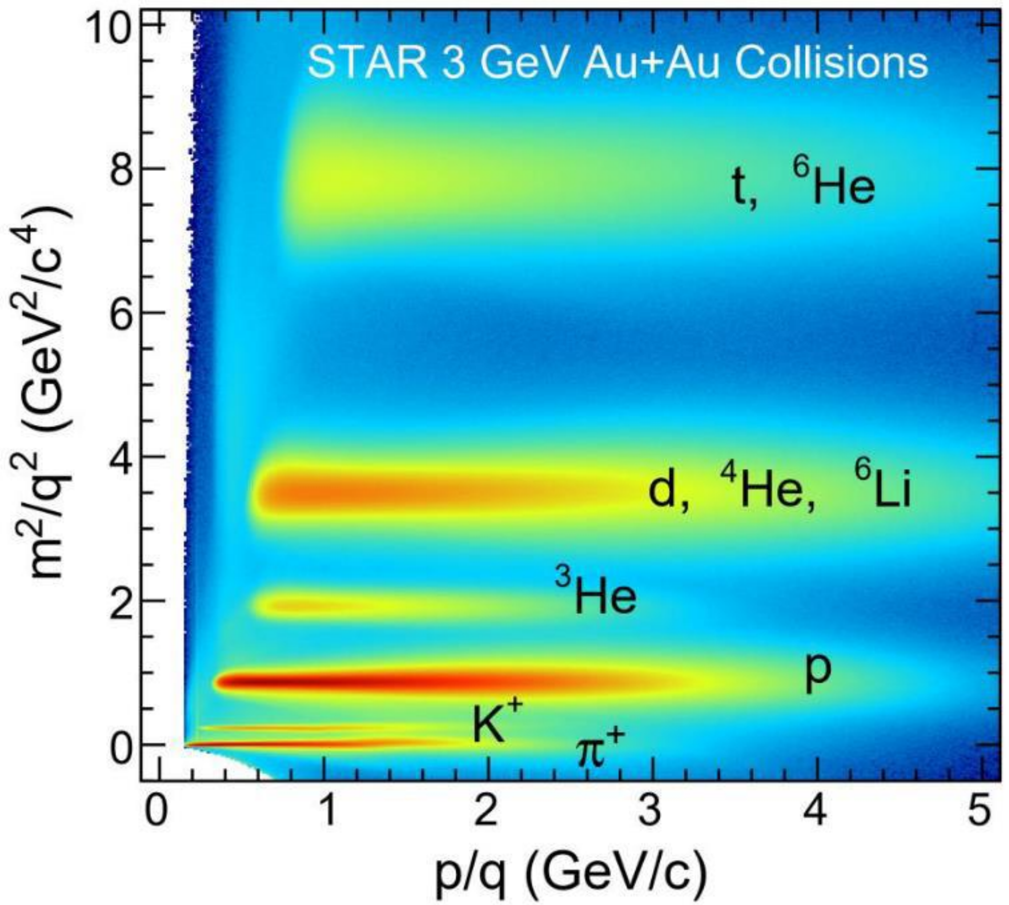

Good particle identification in a broad momentum range using TPC and TOF

Detects particles in the $0 < \eta < 2$ range
π, K, p, d, t, h, α through dE/dx and ToF
K^0_s, Λ, Ξ, Ω, φ, ${}^3_\Lambda H$, ${}^4_\Lambda H$ trough invariant mass

About 260M events analyzed from 2018,
2B more recorded in 2021

Two pion femtoscopy results from FXT program

Anna Kraeva, Fr. 09:20 AM
Vinh Luong, Fr. 09:40 AM

Bowler-Sinyukov procedure:

$$C(q) = N[(1-\lambda) + \lambda K(q)(1+G(q))] \text{ , where}$$
$$G(q) = \exp(-q_{out}^2 R_{out}^2 - q_{side}^2 R_{side}^2 - q_{long}^2 R_{long}^2 - 2q_o q_l R_{ol}^2)$$

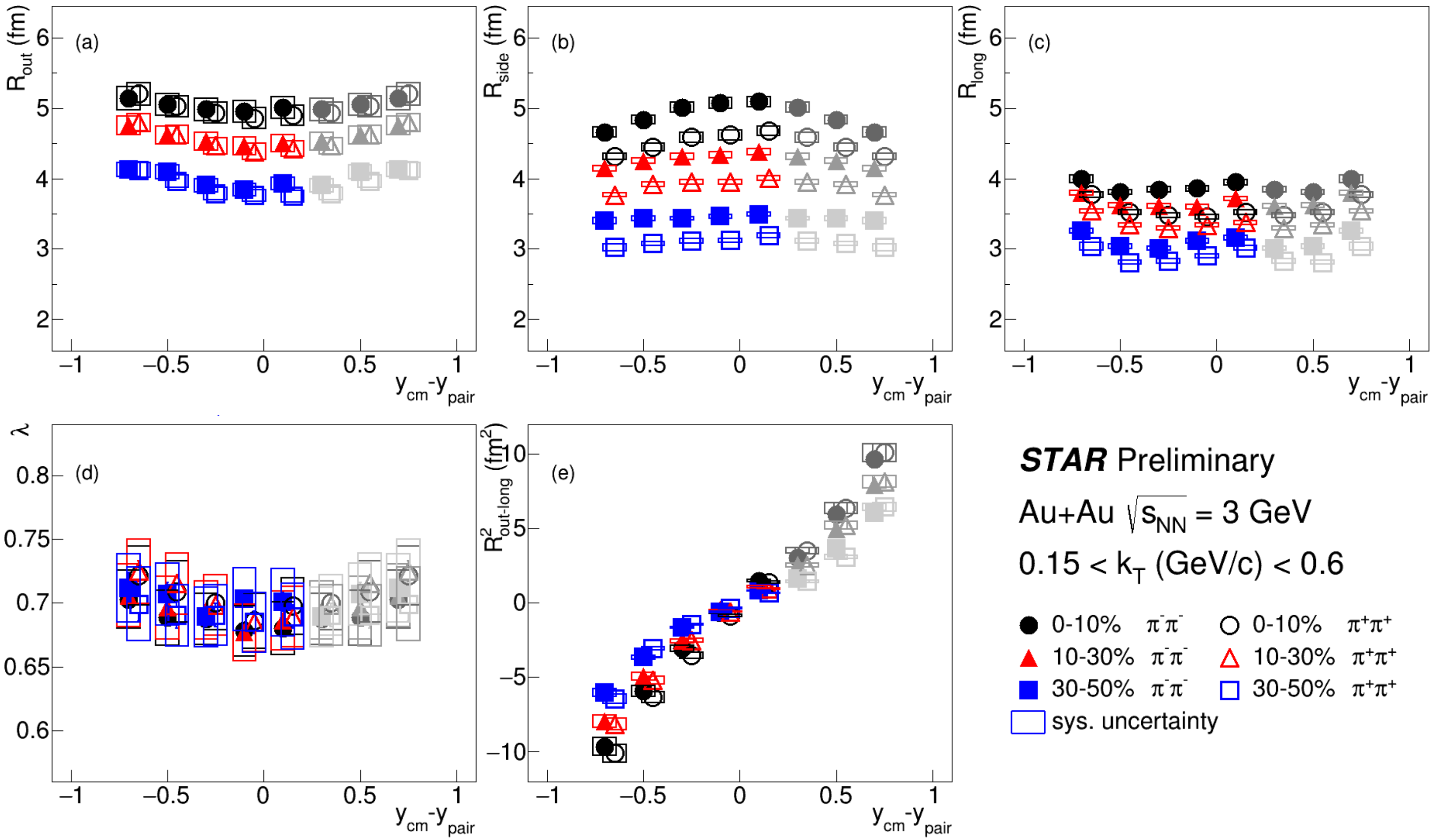

N - normalization factor,
K(q) - Coulomb correction factor,
λ - correlation strength,
R_{side} ~ geometrical size of the particle emission source,
R_{out} ~ geometrical size + particle-emitting duration
R_{long} ~ medium lifetime,
$R^2_{out\text{-}long}$ – tilt of the CF in the q_{out} — q_{long} plane, depending on the degree of asymmetry of the rapidity acceptance w.r.t. midrapidity.

- R_{out}, R_{side} and R_{long} increase from peripheral to central collisions reflecting the geometry of the overlapping region.
- R_{side} decreases with going out of midrapidity:
  Hints on boost-invariance breaking.

Two pion femtoscopy results from FXT program

Vinh Luong
Friday 09:40 AM

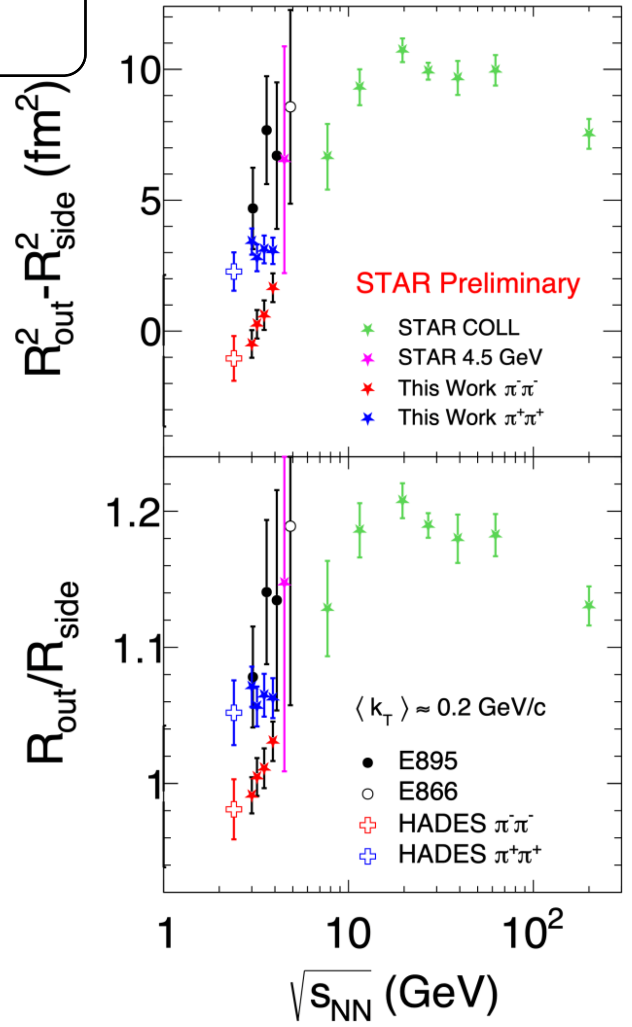

The source shape evolves from oblate to prolate, as energy increases

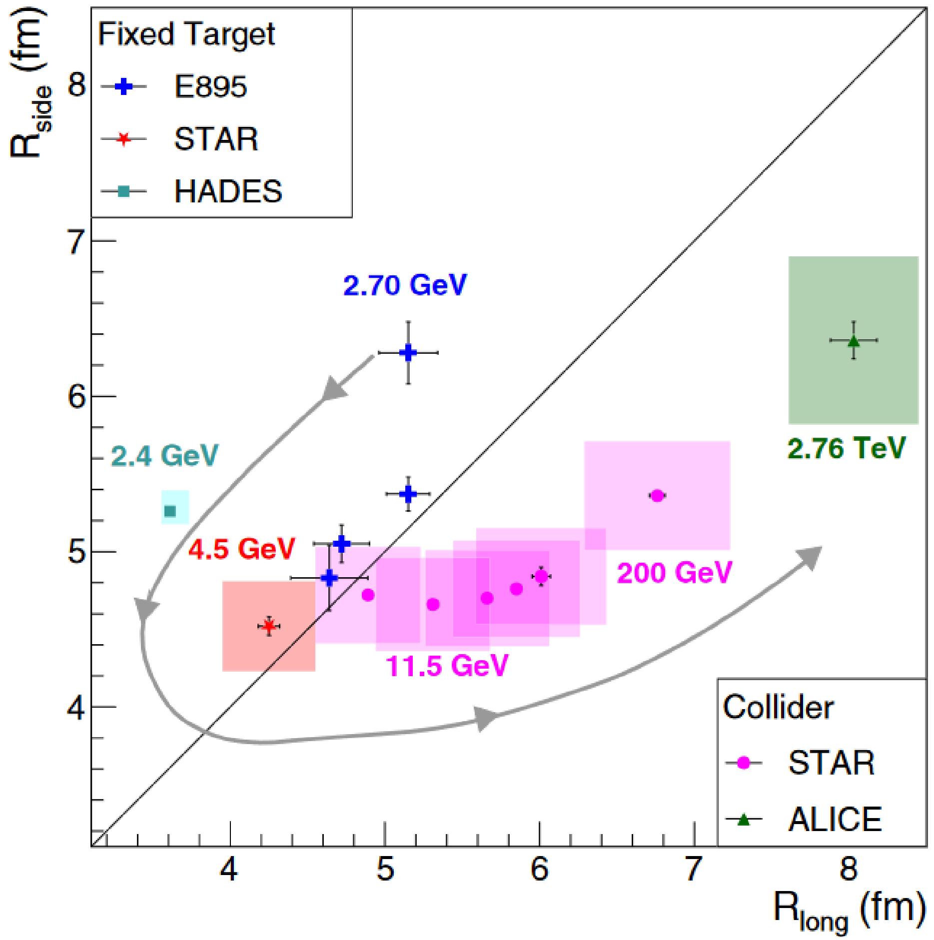

STAR. PRC 103, 034908(2021)

- Extracted parameters and $R^2_{out} - R^2_{side}$, R_{out}/R_{side} ratios at $\sqrt{s_{NN}}$ = 3.0 - 3.9 GeV follow the trend of HADES and STAR's collider mode results.

p-Λ and d-Λ Correlation Measurement in 3 GeV Au-Au collisions

Source Size with L-L approach

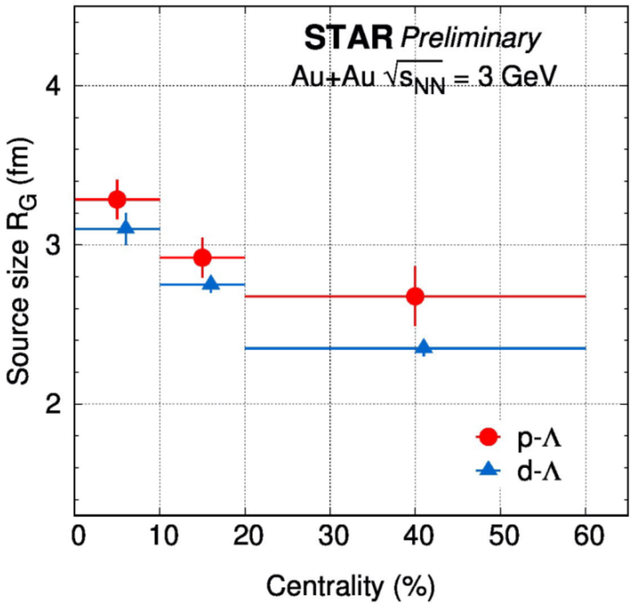

R_G: spherical Gaussian source of pairs by Lednicky-Lyuboshits (L-L) approach

- Separation of emission source from final state interaction

Collision dynamics as expected:

$R_G^{central} > R_G^{peripheral}$ and $R_G\,(p-\Lambda) > R_G\,(d-\Lambda)$

R. Lednicky, et al. Sov.J.Nucl.Phys.35(1982)770
L. Michael, et al. Ann.Rev.Nucl.Part.Sci. 55 (2005)
J. Haidenbauer, Phys.Rev.C 102 (2020) 3, 034001

Scatterings Length (f_0) and Effective Range (d_0)

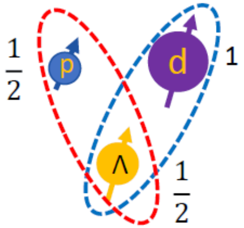

$$\frac{1}{f(k)} \approx \frac{1}{f_0} + \boxed{\frac{d_0 k^2}{2}} - ik$$

❖ The constraint of the effective range (d_0) is weaker

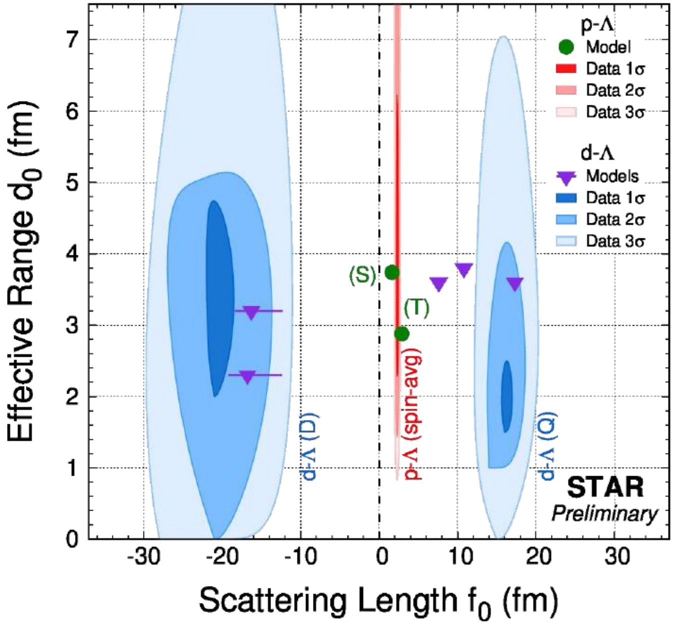

p-Λ correlation spin-ave:

$f_0 = 2.32^{+0.12}_{-0.11}$ fm $\quad d_0 = 3.5^{+2.7}_{-1.3}$ fm

d-Λ correlation spin-sep:

$f_0(\mathrm{D}) = -20^{+3}_{-3}$ fm $\quad d_0(\mathrm{D}) = 3^{+2}_{-1}$ fm

$f_0(\mathrm{Q}) = 16^{+2}_{-1}$ fm $\quad d_0(\mathrm{Q}) = 2^{+1}_{-1}$ fm

$^3_\Lambda$H binding energy (B_Λ):

❖ Bethe formula from Effective Range Expansion (ERE) parameters $f_0(\mathrm{D})$ & $d_0(\mathrm{D})$

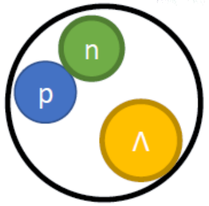

$$\frac{1}{-f_0} = \gamma - \frac{1}{2} d_0 \gamma^2$$

❖ $B_\Lambda = \frac{\gamma^2}{2\mu_{d\Lambda}}$

❖ $\mu_{d\Lambda}$: reduced mass

❖ γ: binding momentum

H. Bethe, Phys. Rev. 76, 38 (1949)

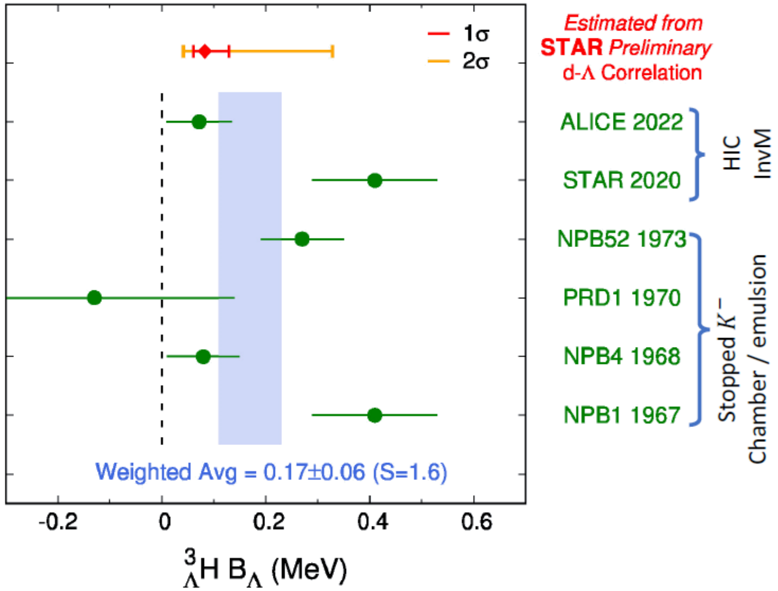

$^3_\Lambda$H B_Λ = [0.04,0.33] (MeV) @ 95% CL

Consistent with the world average

Beam-energy dependence of anisotropic flow fluctuations and correlations

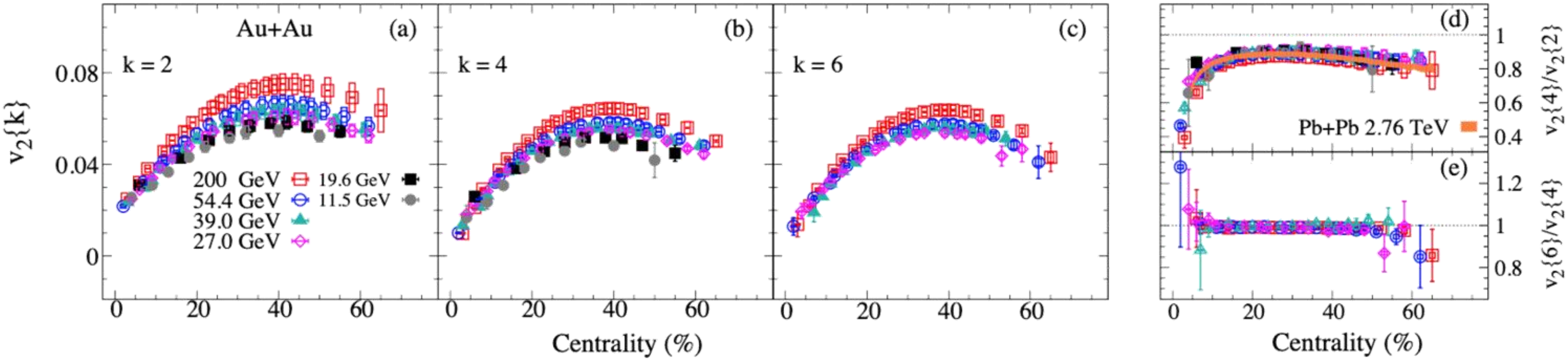

Assuming a Gaussian distribution of v_2

$v_2\{2\} \approx \langle v_2 \rangle + \sigma^2 /(2\,\langle v_2 \rangle)$

$v_2\{4\} \approx v_2\{6\} \approx \langle v_2 \rangle - \sigma^2/(2\,\langle v_2 \rangle)$

$v_2\{4\}/v_2\{2\}$ ratio serves as a metric for v_2 fluctuations

$v_2\{k\}$ increasing with increasing colliding energy

$v_2\{4\}/v_2\{2\}$ show a weak colliding energy dependence

Weak energy dependence of flow fluctuations

$v_2\{6\}/v_2\{4\}$ are consistent with unity within uncertainties

STAR, PRL **129** (2022) 252301

Net-Proton Critical Fluctuations

The results at 3 GeV are consistent with the UrQMD baseline, which is below unity due to baryon conservation.

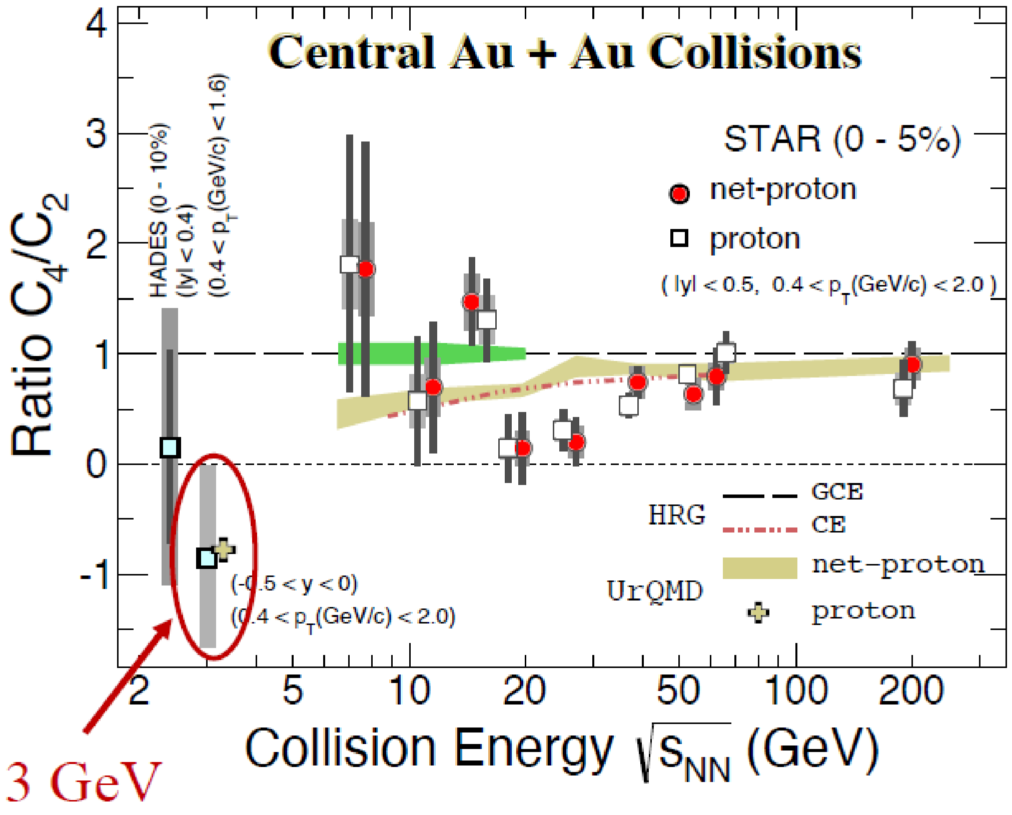

Non-monotonous energy dependence could indicate critical behavior

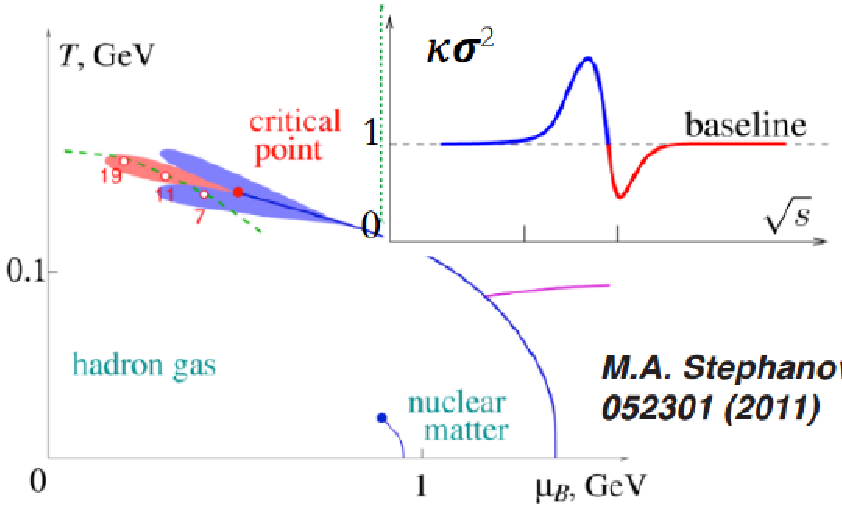

M.A. Stephanov, PRL107, 052301 (2011)

- Net-proton $\kappa\sigma^2$ (C_4/C_2) show a non-monotonic behavior. The trend is consistent with the expectation from theoretical calculations having a critical point.
- Enhancement at low beam energies cannot be explained by baryon number conservation.

STAR, PRL 128 (2022) 202303

Hypernuclei production

Hyper-triton

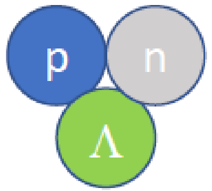

$$ {}^{3}_{\Lambda}H \rightarrow {}^{3}He + \pi^{-} $$

$$ {}^{4}_{\Lambda}H \rightarrow {}^{4}He + \pi^{-} $$

Hyper-^{4}H

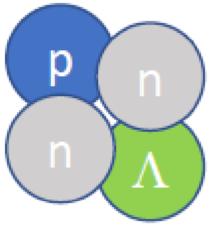

$$ \tau({}^{3}_{\Lambda}H) = 221 \pm 15(stat.) \pm 19(syst.)\ ps. $$

$$ \tau({}^{4}_{\Lambda}H) = 218 \pm 6(stat.) \pm 13(syst.)\ ps. $$

260M Au+Au data without iTPC and eTOF

Candidate reconstruction via invariant mass in two body decay

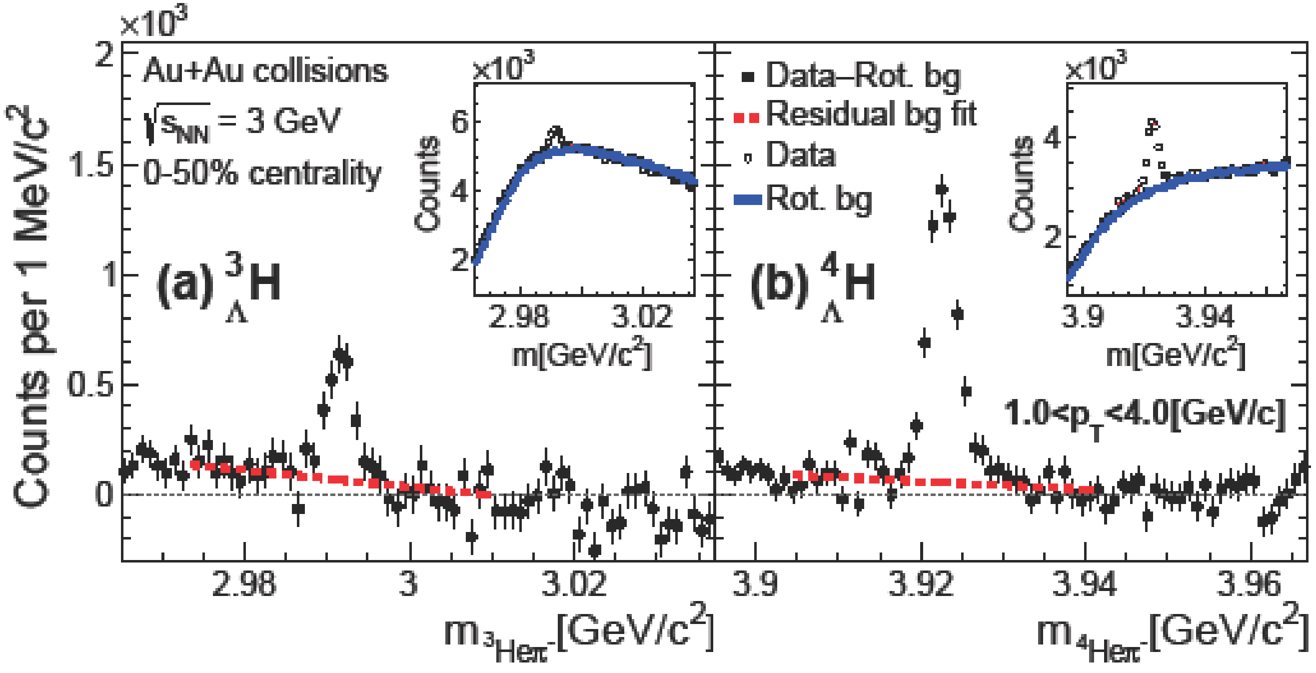

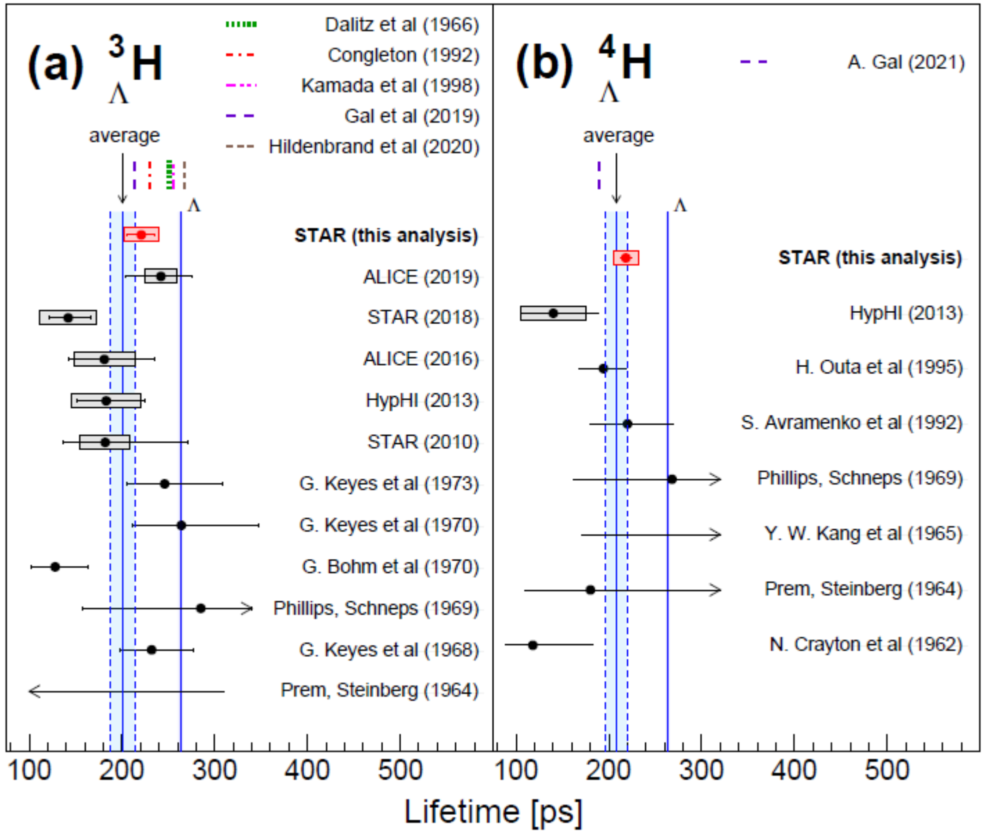

The lifetimes of the two hyper-nuclei are both 20% lower than the free Lambda lifetime.

Phys. Rev. Lett. 128 (2022) 202301

Hypernuclei production

STAR Phys. Rev. Lett. **128,**202301 (2022)
STAR Phys. Rev. Lett. **130**, 211301 (2023)

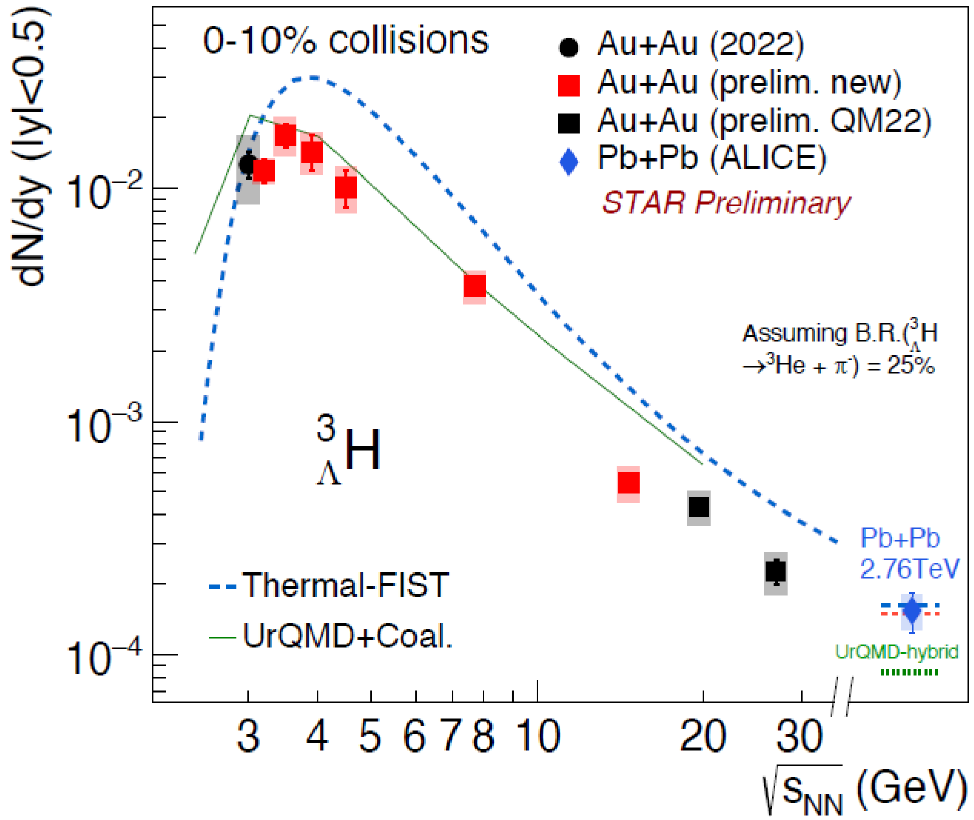

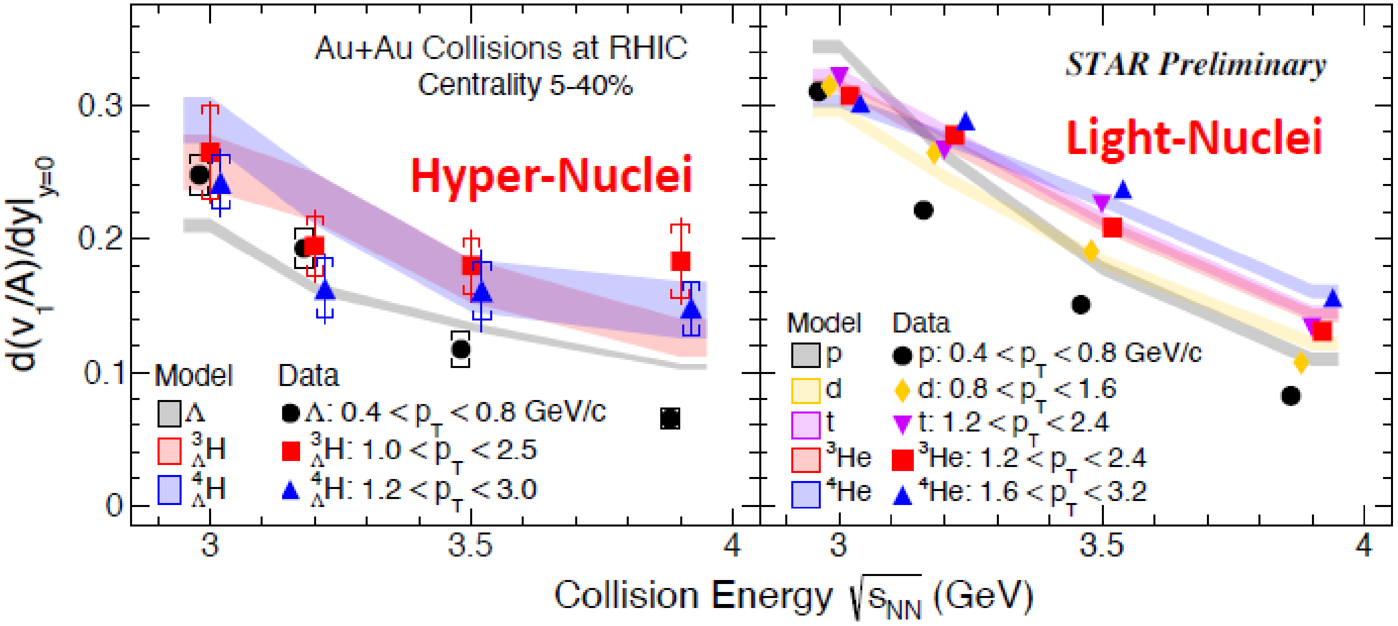

Coalescence calculation consistent with data at 3.5 < $\sqrt{s_{NN}}$ < 10 GeV, while still significantly higher than data at higher energies.

Thermal model fails to describe the trend at RHIC energies.
Hypernuclei maybe dominantly produced after the hadron chemical freeze-out at RHIC.
The slopes of mid-rapidity v_1 for both light-and hyper-nuclei are scaled with A and/or mass across multiple collision energies. v_1 is consistent with hadronic transport (JAM2 mean field + coalescence)

Particle Production at 3 GeV

Spectra and rapidity densities have been measured for:

- π^+
- π^-
- K^+
- K^0_S
- K^-
- ϕ
- P
- Λ
- Ξ
- d
- t
- h
- α
- ${}^3_\Lambda H$
- ${}^4_\Lambda H$
- ${}^4_\Lambda He$

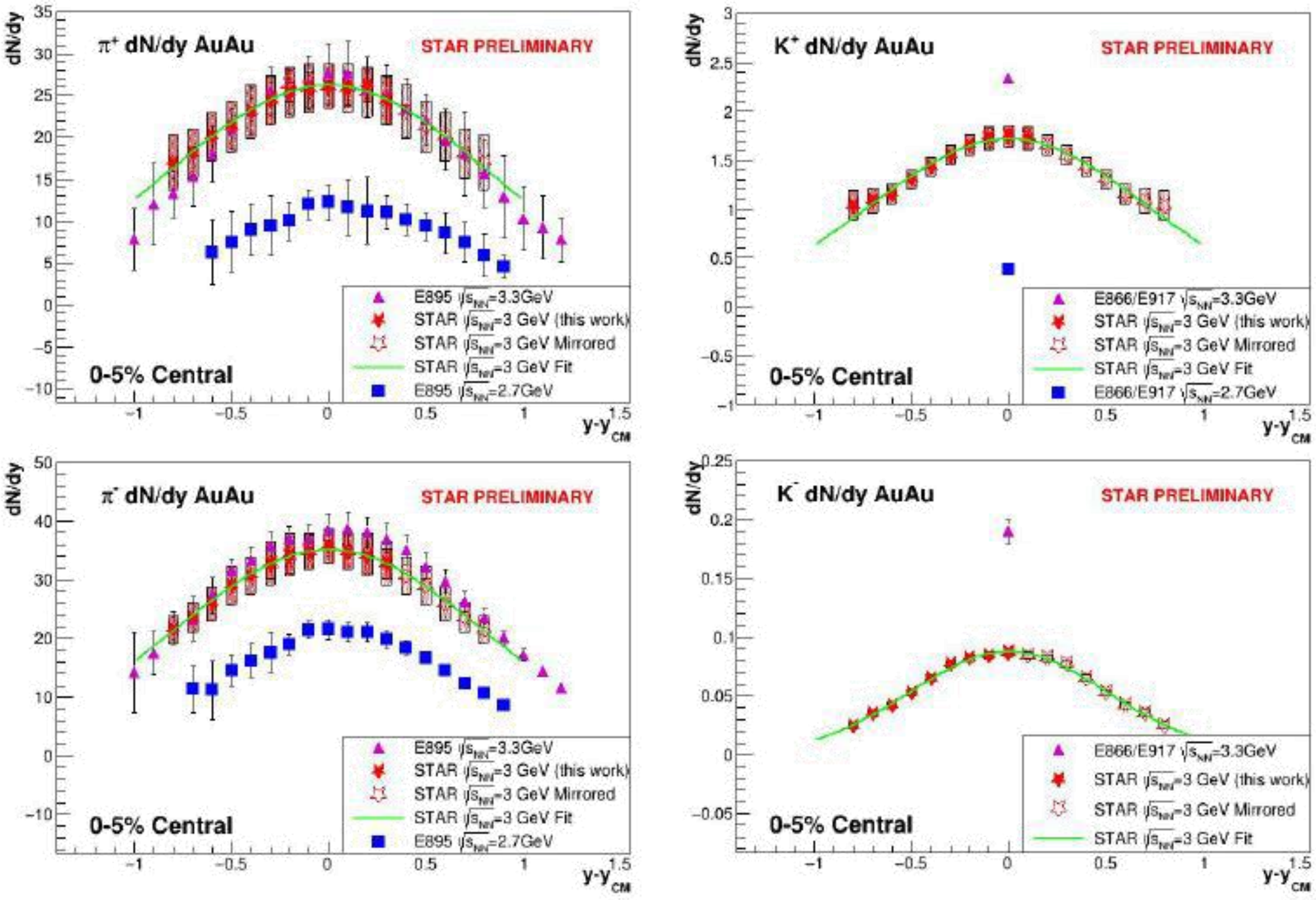

- Spectra require detailed calculations of efficiency, backgrounds and feed-down.
- The low p_T pions are strongly affected by the coulomb potential of the source.
- The charged kaons mostly comes from associated production.
- The Heinz blast wave needs to be modified to work in an environment which is not boost invariant.

Particle Production at 3 GeV

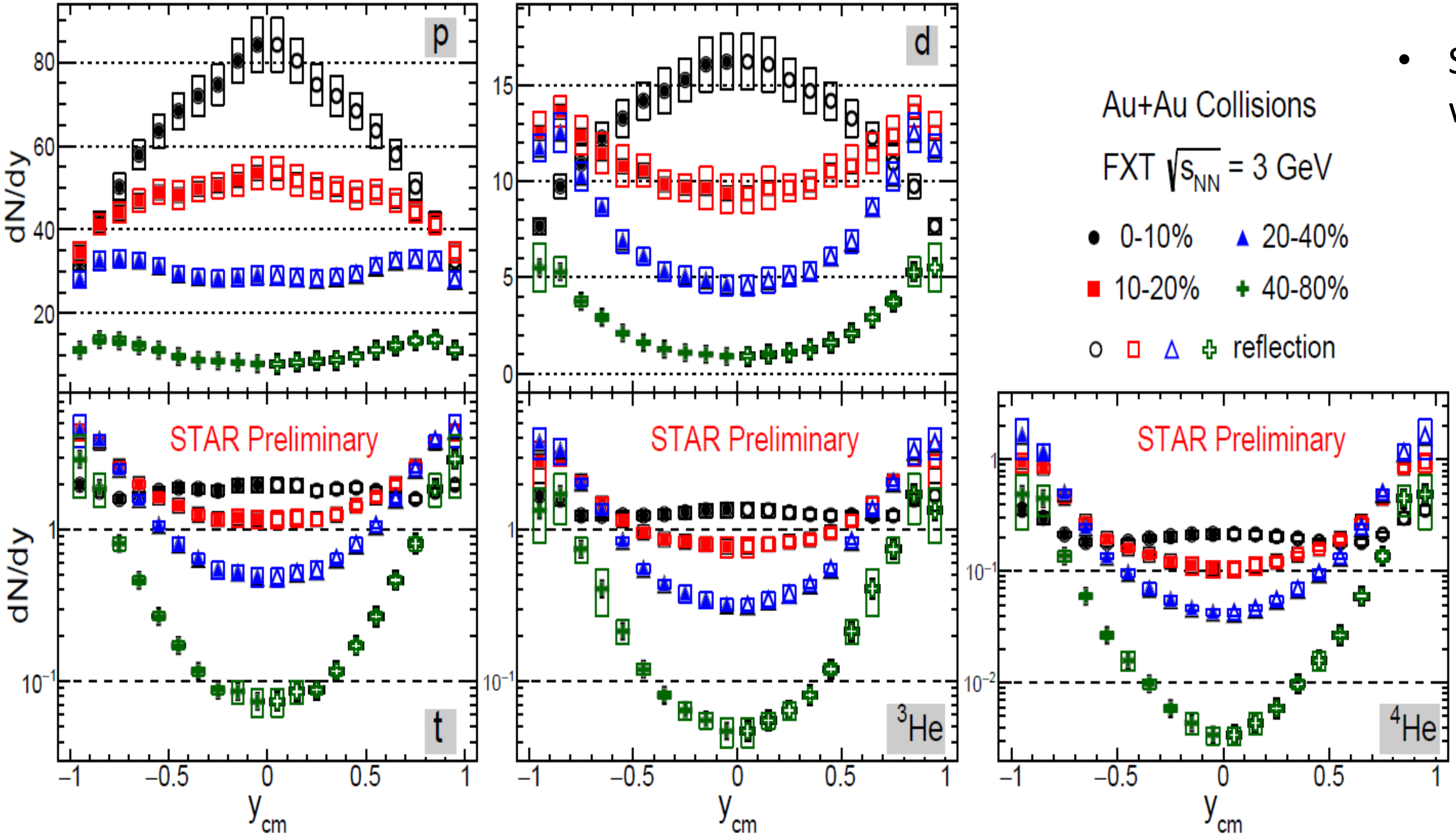

- Strange particle production is not well represented by UrQMD.

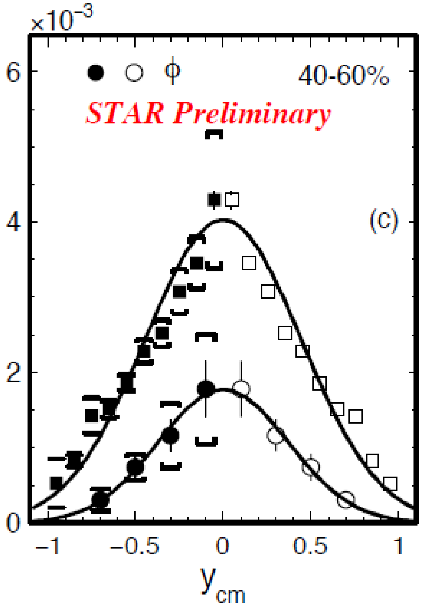

Particle Production at 27 GeV

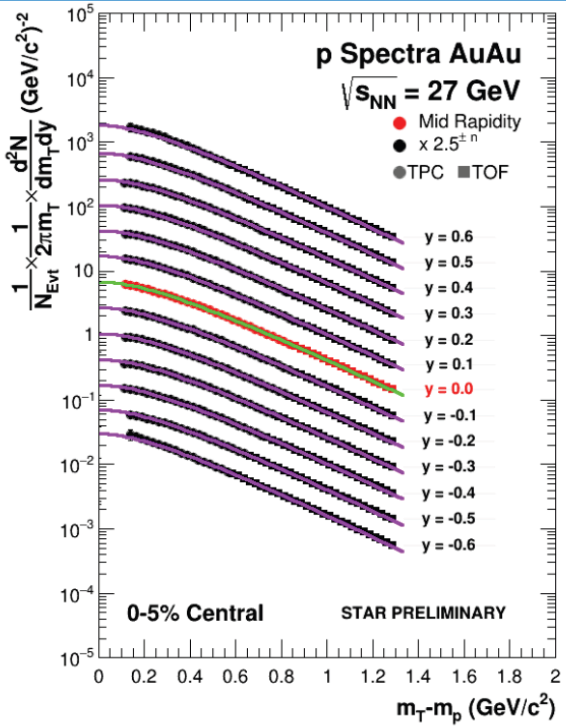

High statistics of BES-II allows to make a rapidity dependence study of particle production

With iTPC and eTOF upgrade more high precision data on particle production are on the way at lower energies

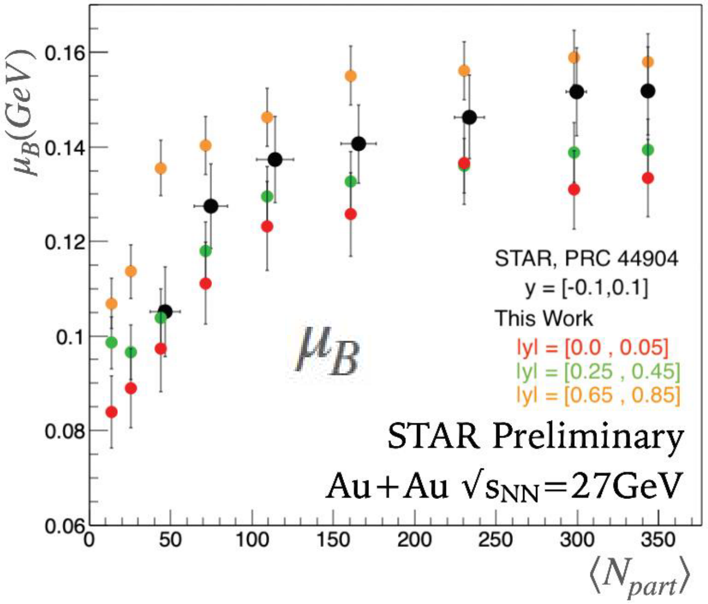

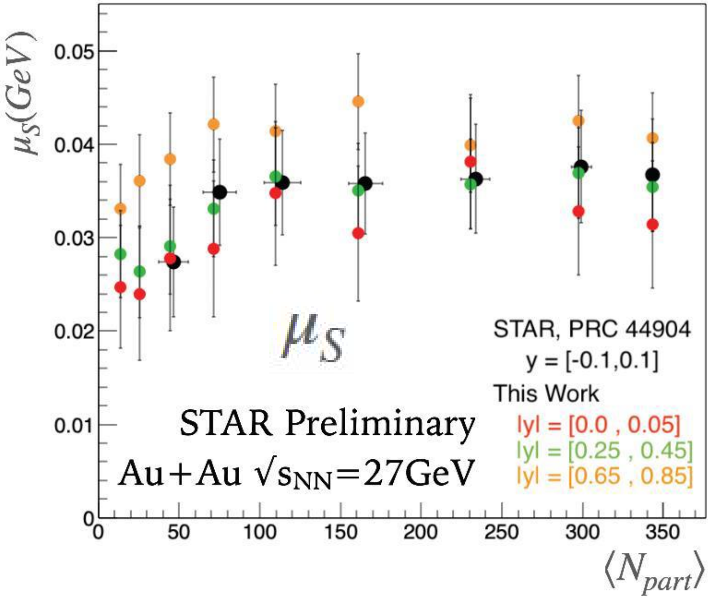

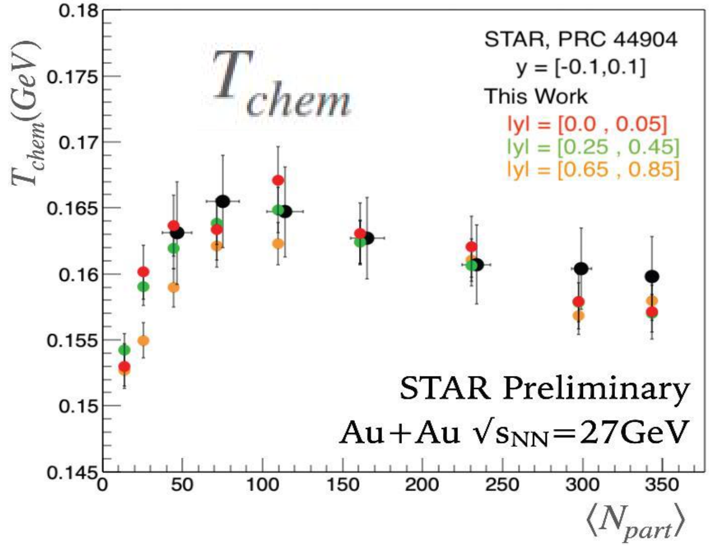

Similar rapidity dependence of the T_{chem} and μ_B, μ_S over particle multiplicity

Precise study of the QCD phase diagram location of the interaction at different collision energies

Fits by THERMUS
- Chemical equilibrium model
- $\Delta\mu_B \approx 25$ MeV for $\Delta y = 1$ at 27 GeV

Global hyperon polarization measurements

Egor Alpatov
Tuesday 04:50 PM

Lambda polarizations are expected to be sensitive to the vortical flow structure of the QGP.

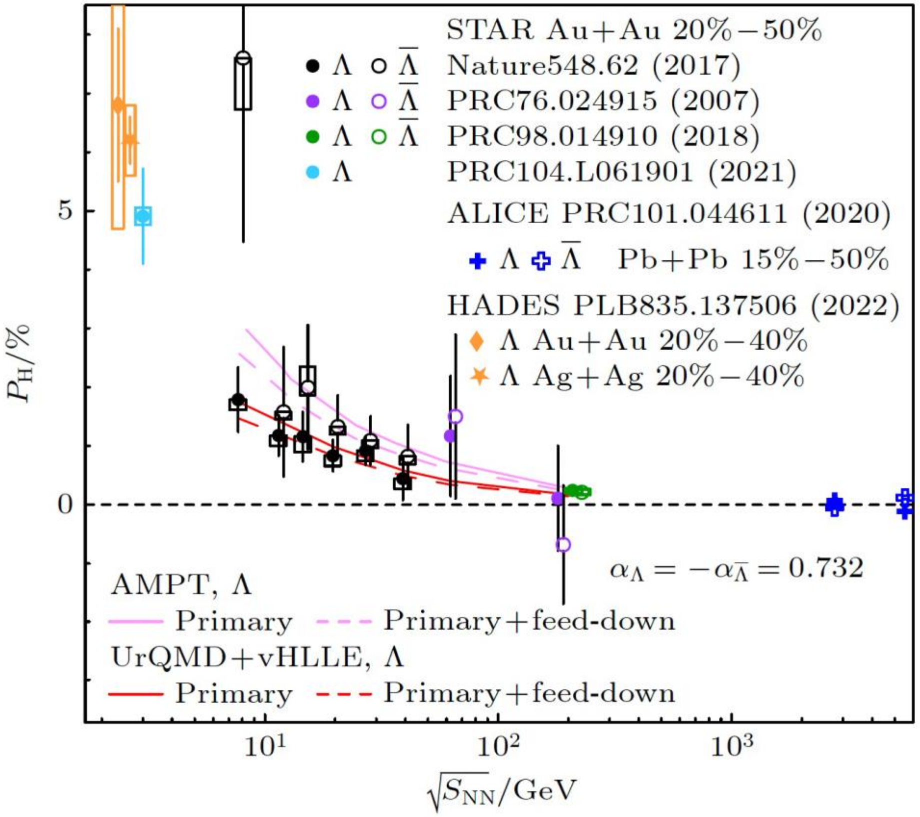

Acta Phys. Sin. Vol. 72, No. 7(2023) 072401

- Significant polarization is seen at 3.0 GeV
- At 19.6 and 27.0 GeV, the Lambda and anti-Lambda polarizations are very similar, placing an upper limit on the late-stage magnetic filed

$$\frac{dN}{d\cos\theta^*} = \frac{1}{2}\left(1 + \alpha_H |\vec{\mathcal{P}}_H| \cos\theta^*\right)$$

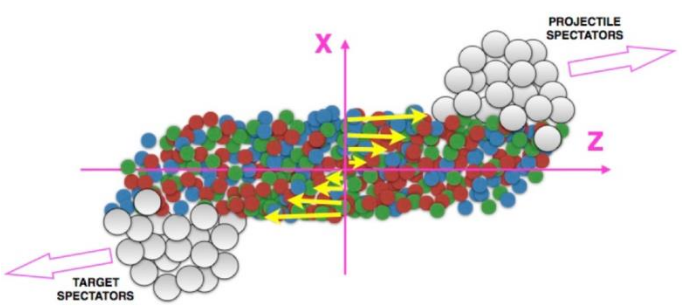

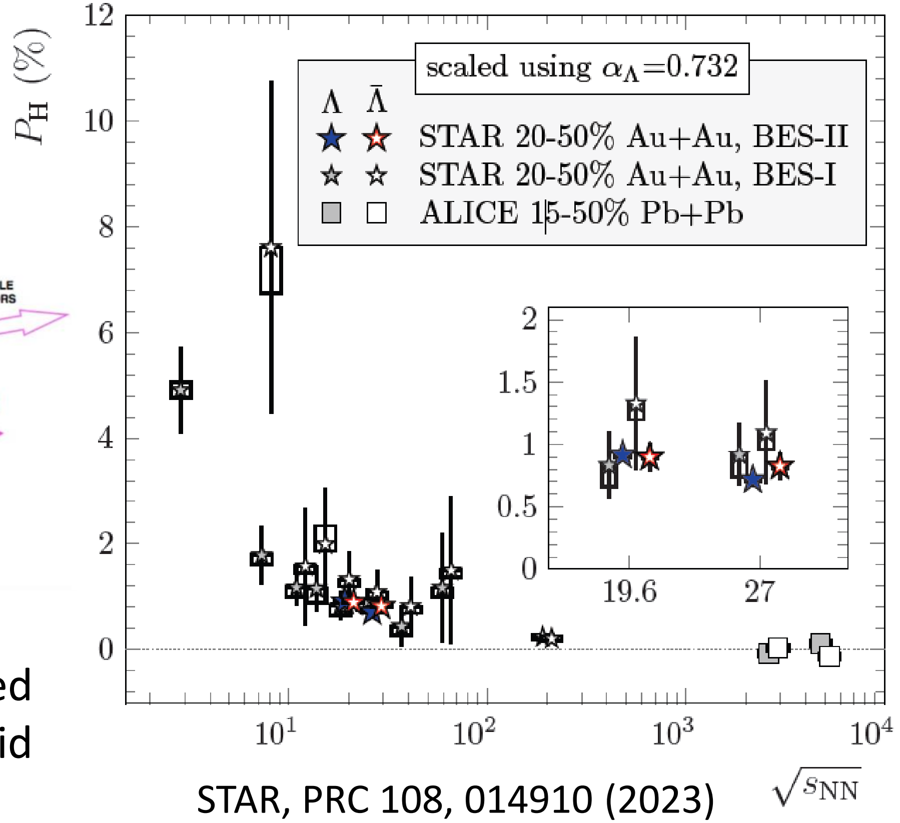

STAR, PRC 108, 014910 (2023)

Global hyperon polarization over a large range of collision energy is measured and can be described by hydrodynamic and transport models with intense fluid vorticity of the QGP

Nuclear modification in the medium

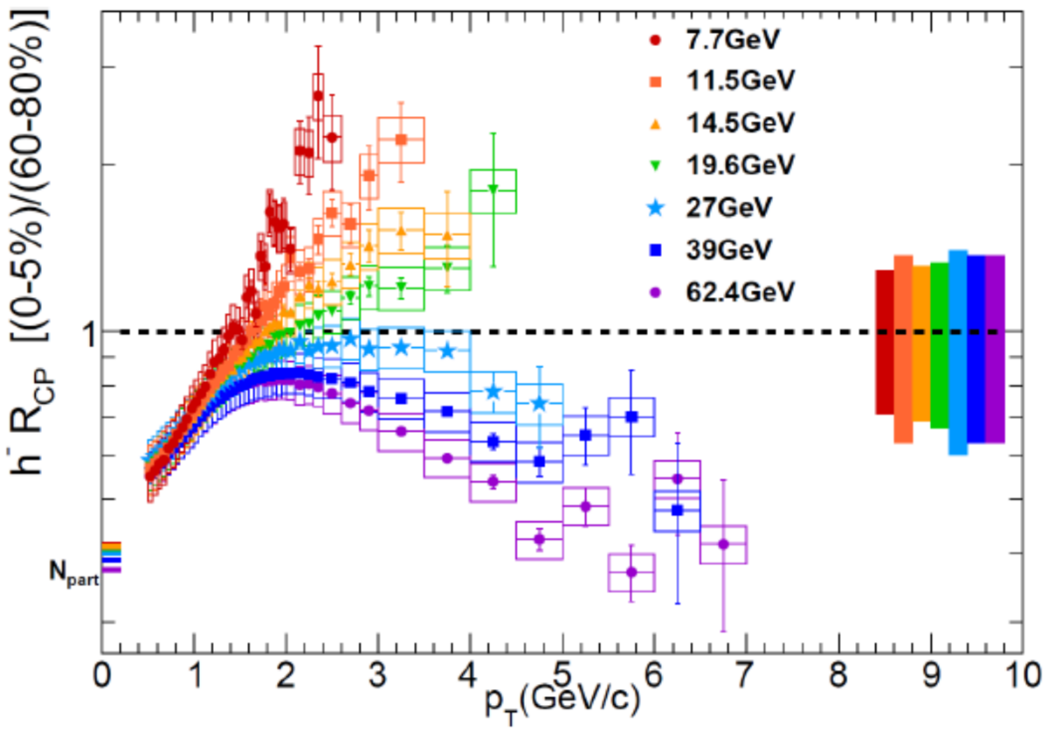

$$R_{cp} = \frac{d^2 N dp_t d\eta / < N_{coll} > (central)}{d^2 N dp_t d\eta / < N_{coll} > (peripheral)}$$

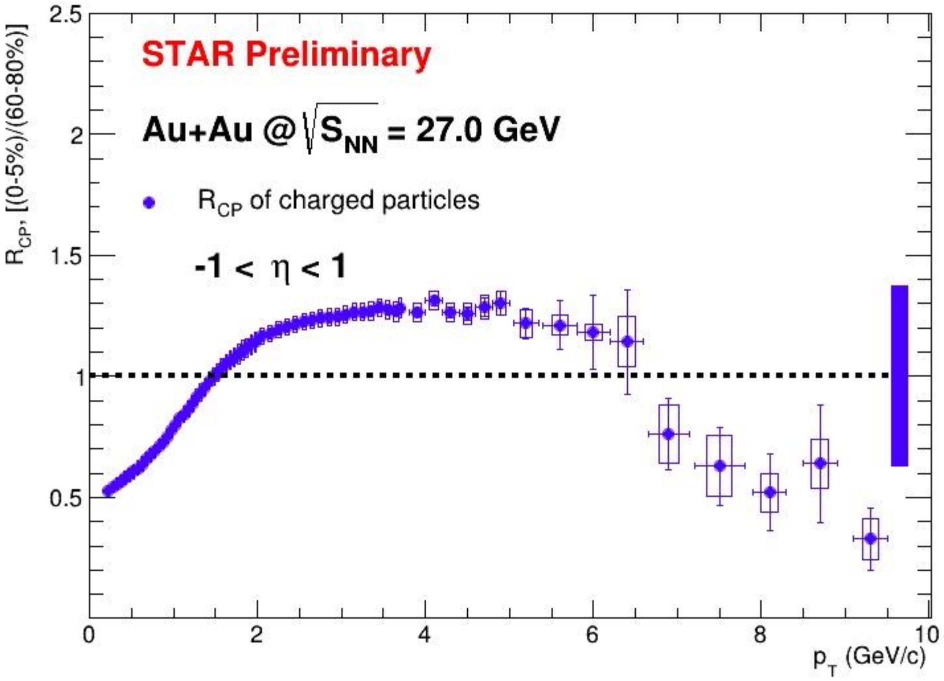

R_{cp} has two regimes in the behavior depending on the collision energy:

- decrease of particle production with high p_T in central collisions at high energies
- smooth growth of particle production in central collisions at low collision energies.

High statistics of BES-II will allow to measure R_{cp} in high p_T region at low collision energies

Phys. Rev. C **102** (2020) 34909
Phys. Rev. Lett. **121** (2018) 32301

Summary

STAR experimental program covers a wide range of topics and STAR has collected a unique set of data on a variety of collision systems and collision energies including fixed target data;

All requested BES II data collected, providing 17 unique energies from 3-200 GeV with some overlapping collider and FXT energies;

BES-II has increased statistics by a factor of 10 for most of the energies and provided additional data with FXT mode of STAR detector;

Run 23 was the 1-st top energy Au+Au with all upgrades. STAR recorded 6.5B events before unexpected RHIC shutdown

Thank you for the attention!

Part of this work was supported by Russian Science Foundation under grant №22-72-10028

BES-II statistics and run time

STAR ☆

Recent BES-II, FXT and 200 GeV datasets (years 2018-2021)

$\sqrt{s_{NN}}$ (GeV)	Beam Energy (GeV/nucleon)	Collider or Fixed Target	$y_{center\ of\ mass}$	μ_B (MeV)	Run Time (days)	No. Events Collected (Request)	Date Collected
200	100	C	0	25	2.0	138 M (140 M)	Run-19
27	13.5	C	0	156	24	555 M (700 M)	Run-18
19.6	9.8	C	0	206	36	582 M (400 M)	Run-19
17.3	8.65	C	0	230	14	256 M (250 M)	Run-21
14.6	7.3	C	0	262	60	324 M (310 M)	Run-19
13.7	100	FXT	2.69	276	0.5	52 M (50 M)	Run-21
11.5	5.75	C	0	316	54	235 M (230 M)	Run-20
11.5	70	FXT	2.51	316	0.5	50 M (50 M)	Run-21
9.2	4.59	C	0	372	102	162 M (160 M)	Run-20+20b
9.2	44.5	FXT	2.28	372	0.5	50 M (50 M)	Run-21
7.7	3.85	C	0	420	90	100 M (100 M)	Run-21
7.7	31.2	FXT	2.10	420	0.5+1.0+ scattered	50 M + 112 M + 100 M (100 M)	Run-19+20+21
7.2	26.5	FXT	2.02	443	2+Parasitic with CEC	155 M + 317 M	Run-18+20
6.2	19.5	FXT	1.87	487	1.4	118 M (100 M)	Run-20
5.2	13.5	FXT	1.68	541	1.0	103 M (100 M)	Run-20
4.5	9.8	FXT	1.52	589	0.9	108 M (100 M)	Run-20
3.9	7.3	FXT	1.37	633	1.1	117 M (100 M)	Run-20
3.5	5.75	FXT	1.25	666	0.9	116 M (100 M)	Run-20
3.2	4.59	FXT	1.13	699	2.0	200 M (200 M)	Run-19
3.0	3.85	FXT	1.05	721	4.6	259 M -> 2B(100 M -> 2B)	Run-18+21

BES-I (years 2010, 2011, 2014)

$\sqrt{s_{NN}}$ (GeV)	No. of events (million)
7.7	4
11.5	8
19.6	17.3
27	33
39	111

TPC coverage at FXT energies (Beam Energy (GeV/nucleon))

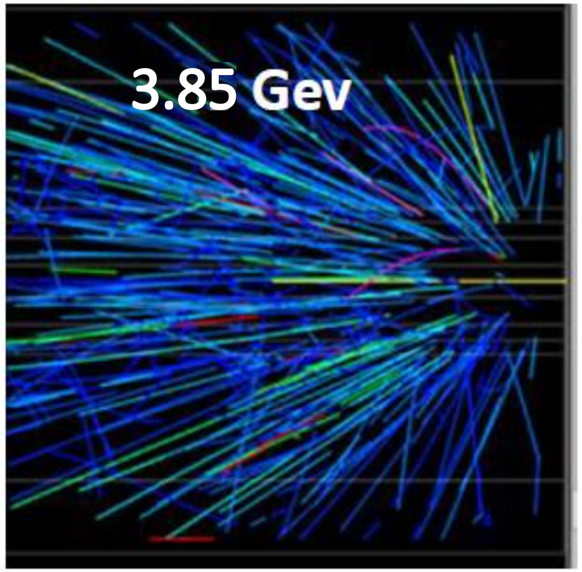

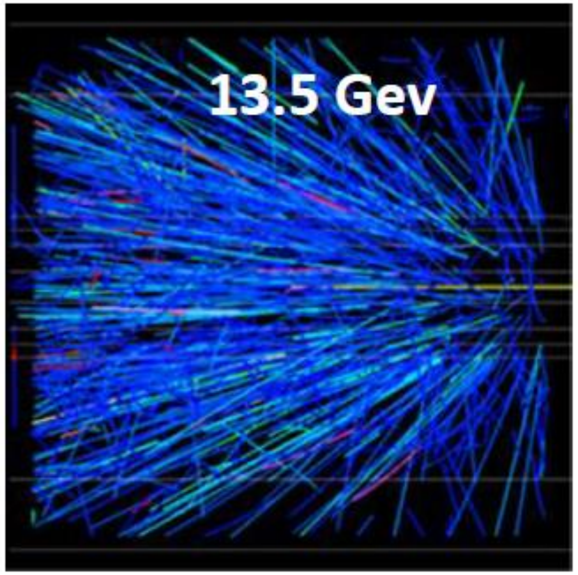

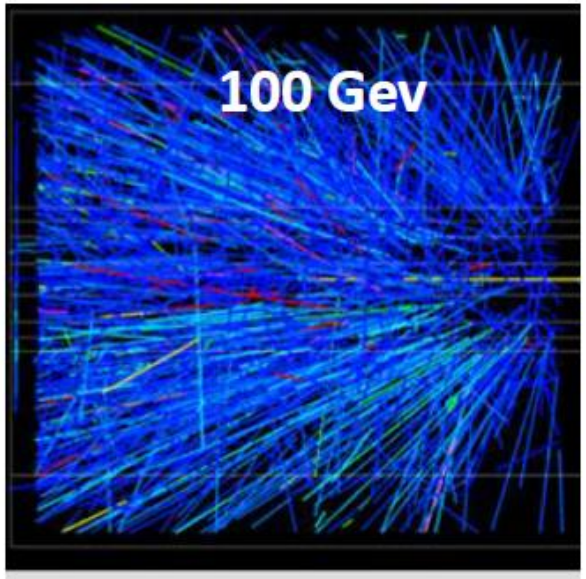

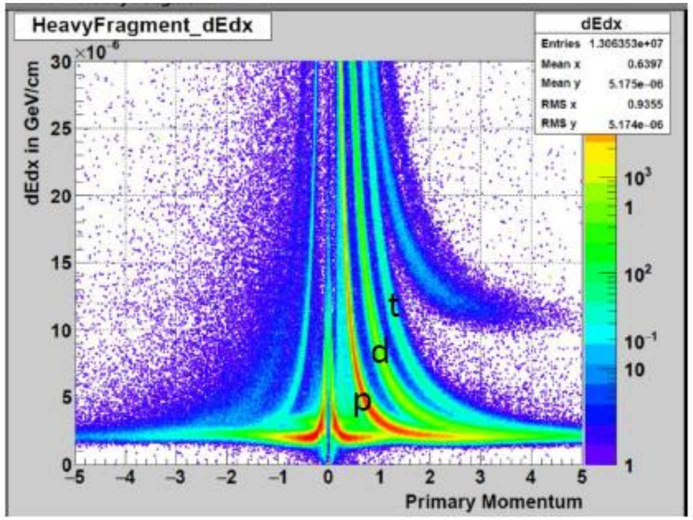

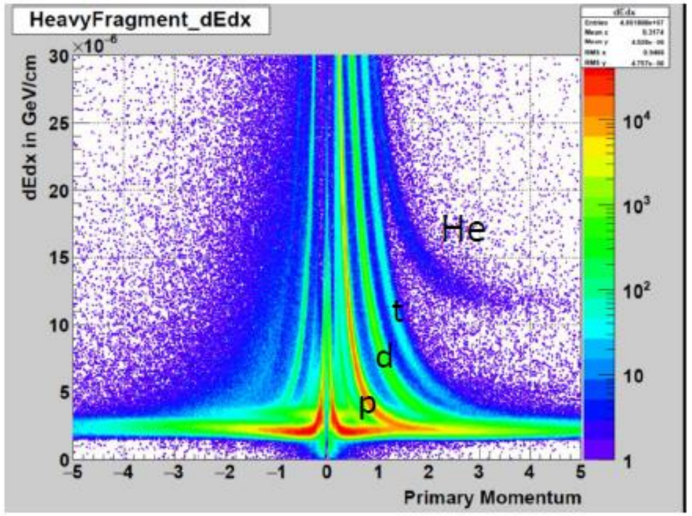

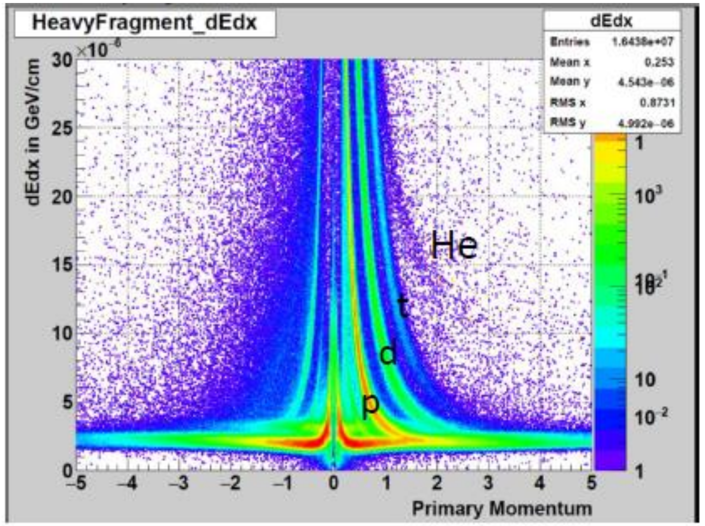

Global hyperon polarization measurements

Egor Alpatov
Tuesday 04:50 PM

Lambda polarizations are expected to be sensitive to the vortical flow structure of the QGP.

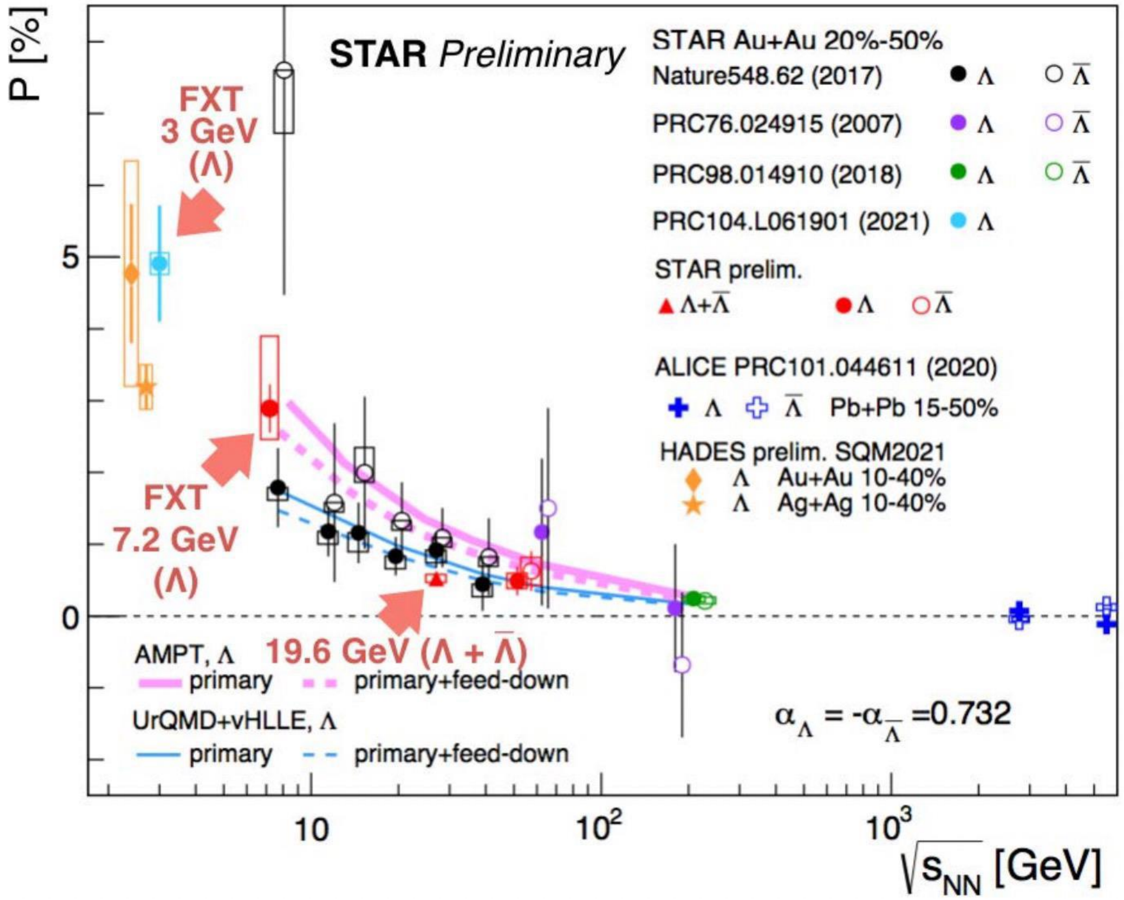

Significant polarization is seen at 3.0 GeV.
At 19.6 and 27 GeV, the Lambda and anti-Lambda polarizations are very similar, placing an upper limit on the late-stage magnetic filed.

Global hyperon polarization over a large range of collision energy is measured and can be described by hydrodynamic and transport models with intense fluid vorticity of the QGP

The observation of substantial polarization in these collisions may require a reexamination of the viscosity of any fluid created in the collision, of the thermalization time scale of rotational modes, and of hadronic mechanisms to produce global polarization.

$$\frac{dN}{d\cos\theta^*} = \frac{1}{2}\left(1 + \alpha_{\mathrm{H}}|\vec{\mathcal{P}}_{\mathrm{H}}|\cos\theta^*\right)$$

Nature 548 (2017) 62,
PRC **104**(2021) 061901,
arXiv: 2204.02302